INFRARED THERMOGRAPHY APPLIED TO CERAMIC MATERIALS: NUMERICAL ANALYSIS AND EXPERIMENTAL RESULTS

Fernando López Rodríguez, flopez@cwpanama.net
Vicente de Paulo Nicolau, vicente@emc.ufsc.br
Eduardo Bonin, bonin@labcet.ufsc.br
Mechanical Engineering Department, Federal University of Santa Catarina, Florianopolis, Brazil

Abstract. *In this work is studied the application of infrared thermography as a technique of non-destructive test on ceramic materials. A transient regimen process is imposed to the ceramic sample, which starts from an elevated and uniform temperature, suffering later a cooling process through the time, as similarly occurs when the sample leaves a furnace. Surface thermal images of the sample are collected during the cooling process using an infrared camera. The presence of defects located either in the interior or in the sample surface will show up in the thermal images and its detection characterizes the availability of this technique as a non-destructive test. A numerical model is used to simulate various kinds of internal defects in the sample test, observing the results that appear in the sample surface and more specifically, the radiant heat flux that is detected by the infrared camera. The numerical solution of the model have been developed using the Finite Volume Method, in which its approximated equations were obtained through the performing of energy balances on each elementary volumes. The thermal response of the cooling process was analyzed and compared with the results obtained numerically. At the same time, other parameters were analyzed such as the induced heat flux, the heating time and the cooling time of the sample, with the purpose of obtaining the best result as possible.*

Keywords: *thermal non-destructive test, thermal simulation, infrared thermography*

1. INTRODUCTION

Even though its use is limited principally because of the high equipment costs, Infrared Thermography (IRT) is a powerful tool which technologic advances and applications scope have increased greatly in the last years, mainly in the Non-Destructive Test field (NDT).

Infrared Thermography as a NDT, is a non-contact and real-time sensing method that provides the surface temperature through the measurement of the infrared radiation emitted by a surface. When the heat flux of a material is altered by the presence of defects or any anomalies, alterations or contrasts in the temperature field appear in the surface. The use of IRT as a NDT method is mainly based on the acquisitions and analysis of those thermal patterns, well known as thermograms.

IRT is deployed along two scheme; passive and active thermography. In the passive thermography scheme, no external stimulation of heating or cooling is employed in order to create a heat flux on the material. Meanwhile, on the active thermography scheme, an external stimulation is induced on the material to produce an internal heat flux. Subsurface defects will affect the heat diffusion rate, producing then a thermal contrast on the surface being tested.

Despite the detection efficiency have increased principally because of the performance of the equipments and the contributions provided by the computer (specifically imaging systems), the defect characterization procedures and the applications of IRT techniques to other materials constitute a wide field of study. At the same time have been dedicated efforts to develop mathematical models together with numerical approach capable to describe the heat transfer process and the interaction of the thermal behavior of the defect, results that would permit compare with those obtained experimentally. Susa et al (2007) make a brief summary of various simplifications and methods (analytical and numerical) employed to find a solution of the heat transfer problem, as well as modeling complex structures samples.

Quantitative Infrared Thermography (QIRT) requires a pre-analysis of the experiment. This is called "direct problem" that consists in "predicting" the thermal behavior of the surface under consideration thought the solution of the mathematical model that describes the phenomenon, aided by numerical and analytical approaches (Maldague, 2001). This pre-analysis provides the possibility to have an estimate of the effectiveness of the procedures, considering variants such as geometry, defect types and characteristic associated to the transient regimen process, making possible to determine its ability to detect without the expense of making tests, often laborious and expensive.

A variety of models have been developed to obtain theoretical results of an IRT test resulting very interesting those presented by (Jena e Sarbahai, 2006) and (Susa et al, 2007) because its similarity with the present work. Jena and Sarbahai (2006) utilizes the analogy between electrical and thermal quantities in the form of electro-thermal models for the simulation of a pulsed thermography test in 1-D, 2-D, e 3-D. The conduction problem 1-D is modeled dividing the material in small parts. Each element has its corresponding equivalent resistance (R) and capacitance (C), values obtained through the fundamental conduction laws of heat and electricity. Similar process is then made for 2-D and 3-D cases. One important feature of this work is the possibility of modeling anisotropic materials, as many materials are.

On the other hand, Susa et al (2007) propose a methodology for the use of pulsed thermography on compound structures, basing on the solution of the transient heat conduction equation, providing the theoretical result of the temperature evolution that comes out during a pulsed thermography test.

In this work we will focus in the application of IRT in ceramic materials using the active thermography approach. The mathematical model proposed is based on the 3-D transient heat conduction equation, which describes the thermal behavior in the interior of the sample and the response due to the external stimulation. At the same time, are considered the thermal losses by convection and radiation that the sample will suffer when exposed to a cooling process at ambient temperature. The resulting temperature field of the surface will be analyzed

As method of validation of the theoretical results, were practiced tests with a ceramic red brick, which was heated inside a kiln at different temperatures. The sample tested containing defects of various diameters and depths, was exposed to transient cooling process, from which thermal images are acquired. The sequences of thermograms of the surface on analysis were obtained using an infrared camera FLIR (TermoCamSC500). Will be studied and analyzed the thermal response of the materials at different external stimulations and how defects interact with the heat flux. Also, will be discussed detection capability and limits of different kinds of defect and depths throughout contrast evolution curves and profiles shapes of the defective zones.

2. MATHEMATICAL MODELLING

The mathematical model proposed in this work that describes the physics of the heat transfer process during a non-destructive test by infrared thermography is given by the Eq. (1):

$$\frac{\partial(\rho T)}{\partial t} = \frac{\partial}{\partial x}\left(\frac{k}{Cp}\frac{\partial T}{\partial x}\right) + \frac{\partial}{\partial y}\left(\frac{k}{Cp}\frac{\partial T}{\partial y}\right) + \frac{\partial}{\partial z}\left(\frac{k}{Cp}\frac{\partial T}{\partial z}\right) \tag{1}$$

Imposing a transient cooling process to the sample, from a high and uniform temperature T_o, the initial condition of the problem is given by the Eq. (2):

$$T(x,y,z,t)_{(t=0)} = T_o \tag{2}$$

The boundary conditions, including the heat transfer lost by convection and radiation between the sample surface and the external ambient are described by the Eq. (3):

$$n.(k.\nabla T) = h_{conv}(T_{amb} - T) + \sigma\varepsilon({T_{amb}}^4 - T^4) \tag{3}$$

In this case, $T(x,y,z,t)$ represents the solid temperature, T_{amb}, the ambient temperature, considering that air and the neighborhood being at the same temperature. The surface emissivity is represented by ε and σ is the Stefan-Boltzmann constant. The spatial coordinates are given by x, y and z. The material thermal conductivity is k, being h_{conv} the convection heat transfer coefficient; C_p is the specific heat and t is the time.

2.1. Numerical approach

The numerical solution of the problem was developed through the Finite Volumes Method (FVM). This method consists in integrating over an elementary volume, on space and time, Eq. (1) and Eq. (3), in the conservative form. This way, in the first integration will show up the heat flux on the boundary of the elementary volume, being the equivalent of making a balance of energy (Maliska, 1995). Then, integrating Eq. (1) over the control volume showed in Fig. (1), we obtain the energy balance equation for internal volumes given by:

$$\frac{M_p T_p - M_p{}^o T_p^o}{\Delta t} = \left[\frac{k}{Cp}\frac{\partial T}{\partial x}\bigg|_e^\theta - \frac{k}{Cp}\frac{\partial T}{\partial x}\bigg|_w^\theta\right]\Delta y.\Delta z + \left[\frac{k}{Cp}\frac{\partial T}{\partial x}\bigg|_n^\theta - \frac{k}{Cp}\frac{\partial T}{\partial x}\bigg|_s^\theta\right]\Delta x.\Delta z + \left[\frac{k}{Cp}\frac{\partial T}{\partial x}\bigg|_b^\theta - \frac{k}{Cp}\frac{\partial T}{\partial x}\bigg|_f^\theta\right]\Delta x.\Delta y \tag{4}$$

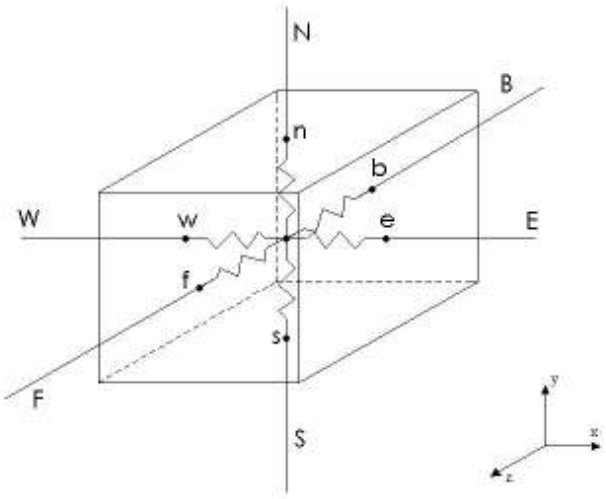

Figure 1. Energy balances for internal volumes

Due to the diffusive nature of the internal heat conduction process within the test sample, the derivatives on the faces of the volume were approximated using central difference scheme as a spatial interpolation function. Likewise, the explicit formulation was used as temporal interpolation function. Substituting the approximation mentioned previously, the energy equation for the internal volumes is given by Eq. (5):

$$\frac{M_p T_p - M_p{}^o T_p^o}{\Delta t} = \frac{k}{Cp}\left[\frac{T_W{}^o - T_P{}^o}{\Delta x} - \frac{T_P{}^o - T_E{}^o}{\Delta x}\right]\Delta y.\Delta z + \frac{k}{Cp}\left[\frac{T_N{}^o - T_p{}^o}{\Delta y} - \frac{T_P{}^o - T_S{}^o}{\Delta y}\right]\Delta x.\Delta z + \frac{k}{Cp}\left[\frac{T_B{}^o - T_P{}^o}{\Delta z} - \frac{T_P{}^o - T_F{}^o}{\Delta z}\right]\Delta x.\Delta y \tag{5}$$

For the boundary condition equation (Eq. 3), integrating on space and time and taken the heat fluxes reference showed in Fig. (2), the approximated energy equation considering the losses by convection and radiation heat transfer, is given by Eq. (5):

$$\frac{q''_{rad}}{Cp}\Delta y.\Delta z + \frac{q''_{conv}}{Cp}\Delta y.\Delta z = \frac{k}{Cp}\bigg|_e \frac{(T_E^o - T_p^o)}{\frac{\Delta x}{2}} \tag{6}$$

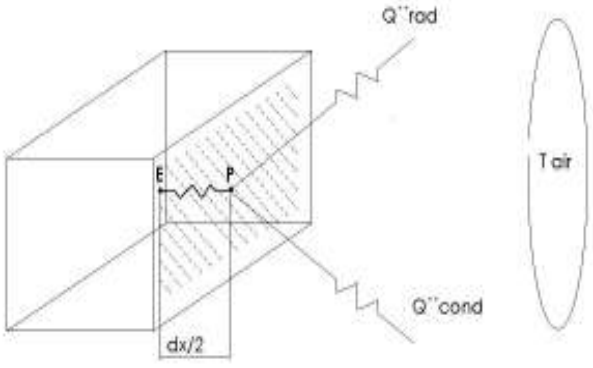

Figure 2. Boundary energy balances

Basing on the mathematical model presented, a computational program was developed on MATLAB for the numerical solution of the temperature field on each of the volume element of the test sample. The program, called THERMOTEST, provides the thermal map of the surface being examinated, in a similar way as is obtained by an

infrared camera. The program also provides important information related to the amount of radiation heat energy that is emitted by the surface and received by the infrared camera during all the cooling process at which the sample is exposed.

2.2. Thermal contrast concept

One of the main approaches for evaluating thermal images in the NDT fields is through the evolution of the thermal contrast on the defective area. The thermal contrast parameter (*C*) provides important information for both qualitative (defect visualization) and quantitative (defect characterization) purposes. When the sample test is exposed to the cooling process, starts the heat diffusion within the material, and also heat transfer by convection and radiation between the sample surface and the external environment. The presence of any defects changes the heat diffusion rate resulting in some spots in the temperature field. Consequently, deeper defect will be observed after and with a reduced contrast. In fact, the observation time *t* is function of the square of the depth *z*, while the loss of thermal contrast *C* is proportional to the cube of the depth, as showed by Eq. (7) (Maldague, 2001), for isotropic materials:

$$t \sim \frac{Z^2}{\alpha} \quad \text{and} \quad C \sim \frac{1}{Z^3} \tag{7}$$

where α is the thermal diffusivity of the medium. These relations indicate two limitations of the IRT: observable defects will generally be shallow and the thermal contrast will be weak. To compute the thermal contrast of a surface, the following expression is used:

$$C(i,j,t) = \frac{\Delta T_{def}(i,j,t)}{\Delta T_{soa}(t)} = \frac{T_{def}(i,j,t) - T_{def}(i,j,t=0)}{T_{soa}(t) - T_{soa}(t=0)} \tag{8}$$

In the Eq. 8, $\Delta T_{def}(i,j,t)$ and $\Delta T_{soa}(i,j,t)$ represent the temperature difference of the defective area and the rest of the surface (called sound area), respectively, in coordinates *i,j*, from an initial time at $t=0$ to any time *t*. This equation is normalized over a non-defect area; a unity value will be obtained over an area without defect if the disturbances from emissivity and thermal reflections stay constant during the experiment.

As it's seen, the temporal evolution of the thermal contrast provides valuable information used to determine parameters of a NDT by IRT. For example, it is possible to have an estimate time at which the defect could be observed better in relation with the rest of the surface analyzed, as well as the defect diameter and depth at which it's located.

3. EXPERIMENTAL SETUP

As it's showed in Fig. (3), the experimental setup consists of the following elements:

1. Infrared camera FLIR (ThermoCam SC500)
2. Data acquisition system with ThermoCam Researcher 2001 software,
3. Electrical 9 KW kilm, 1200 ^{o}C maximum temperature.

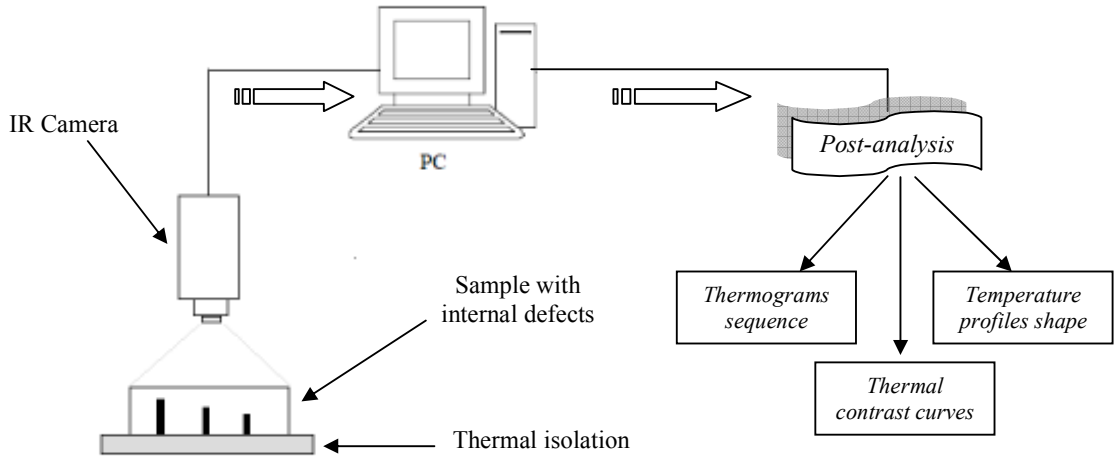

Figure 3. Experimental setup configuration

The sample tested was a solid red brick with geometry and dimension showed in Fig. (4). The sample contains three flat bottom holes at different depth from the surface; the same considerations of geometry and dimensions were used in the simulation program. The sample was heated during a long period at constant temperature by using the kiln in order to get a uniform temperature distribution; this method tries to avoid the non-uniformity of the temperature field that occurs frequently in other stimulation methods. The thermal images capture was made with the surface in horizontal position; otherwise the heat transfer by convection will cause a non-homogeneous distribution of the temperature in the surface being studied. Images acquisitions were made at frequency of 1 FPS.

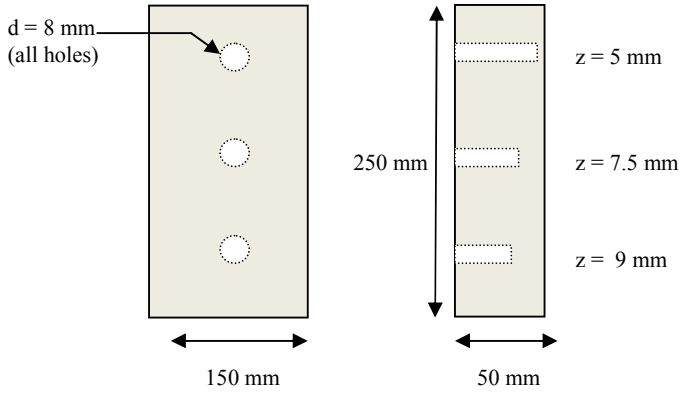

Figure 4. Sample test dimensions and location of the defect

4. RESULTS AND DISCUTIONS

Figure 5 shows a sequence of thermograms obtained by numerical simulation for different defect depths. Was used IR_VIEW (2007) to get the 3D view of the surface temperature distribution in order to see clearly the defects and enhance it visibility. Firstly, it's important to notice that the sound area temperature (sane area) is higher than the defect temperature. That's due to the thermal properties of the defect (specifically the thermal conductivity) which conducts less heat energy than the rest of the body. Using this concept we have now an important key to determine what kind of defect have been detected.

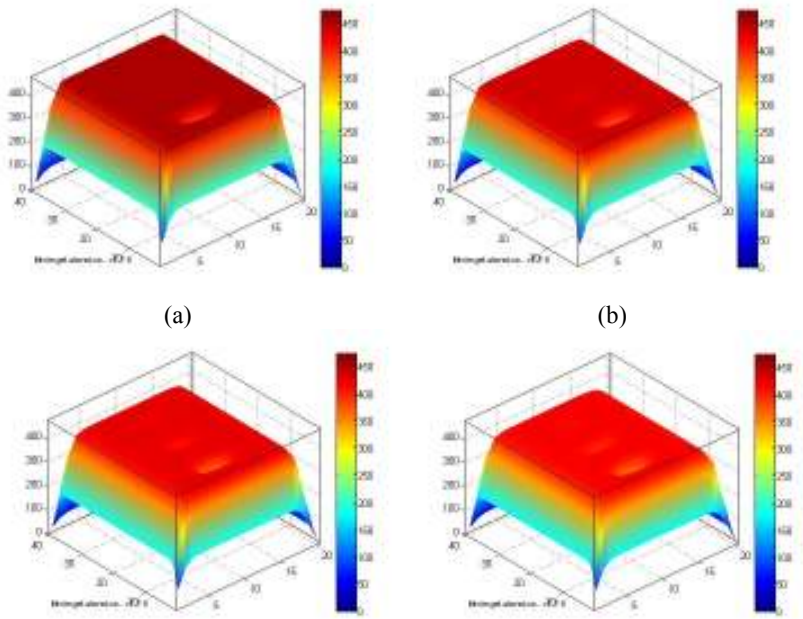

(a) (b)

(c) (d)

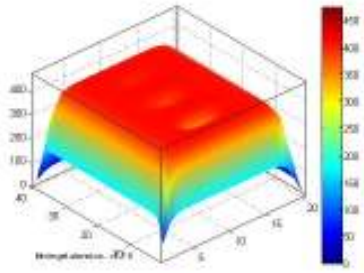

(e)

Figure 5. Sequence of thermograms obtained by numerical simulation corresponding to (a) 5 sec, (b) 25 sec, (c) 50 sec, (d) 75 sec and (e) 100 sec, after the beginning of the cooling process.

The thermogram confirms the scales presented in previous section (Eq. 6); deeper defects are observed later and with a reduced thermal contrast. During all the cooling process, the defect located at 5mm depth is visible, with a higher thermal contrast during the first 25 seconds, as it is showed in Fig. 5a and b. Also in Fig. 5b begins to appear a deeper defect located at 7.5 mm from the surface, which can be clearly seen at 50 seconds from the initial time. A third defect, this at 9 mm depth, can be seen with a weak thermal contrast at 75 seconds (Fig. 5d) and vanishes during the rest of the cooling process.

Another important parameter to analyze is the thermal contrast evolution curve, showed in Fig. 6. These curves, normalized over the sound area, represent quantitatively the time when defects will have the highest thermal contrast. As seem in Fig. 6a and b, the defects will be observable better if the temperature at which the sample test was heated is higher. That's an important key to determine under which heating conditions the defects can be detectable. According to these curves, the defect located at 5 mm from the surface will be better observed at the beginning of the cooling process, reducing its thermal contrast along the time. Quite the opposite occurs when the defects are deep; those defects could only be observable at the final of the cooling process with a weak thermal contrast.

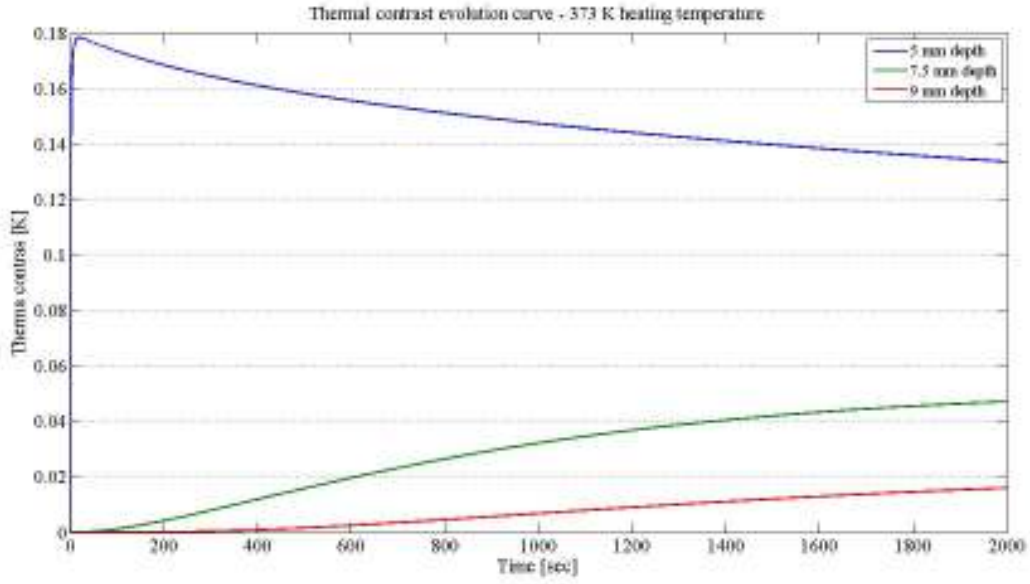

(a)

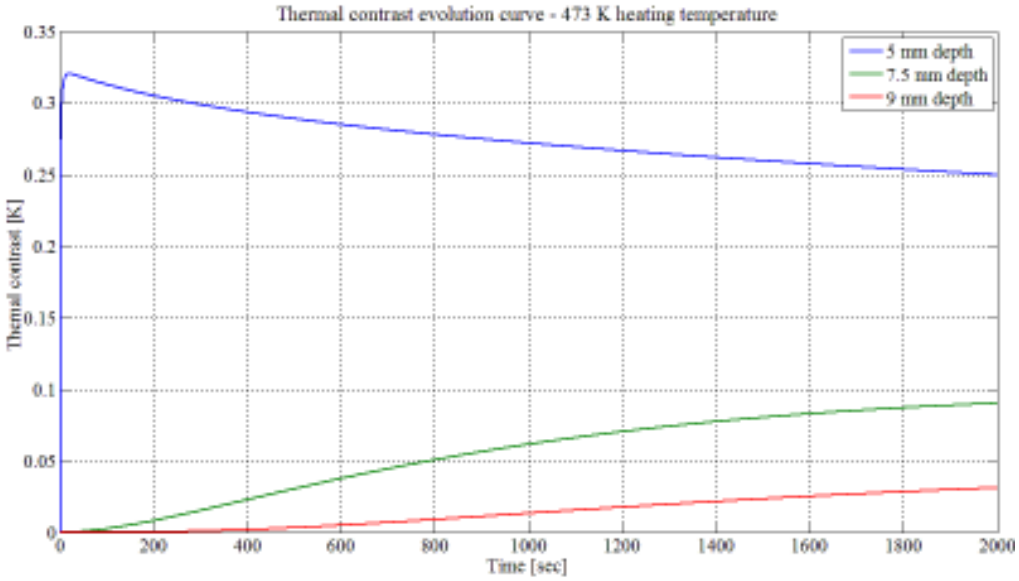

(b)

Figure 6. Thermal contrast evolution curve in time for different heating temperatures

The parameters obtained by numerical simulation were used as starting point for the experimental tests, which results are showed in the Fig. 7. The temperature scale of the thermograms was adjusted so that the images can be compared directly to the results obtained by simulation. In concordance with the theoretical results, the defect located at 5 mm from the surface will first be observable with a strength thermal contrast, which decays along the time.

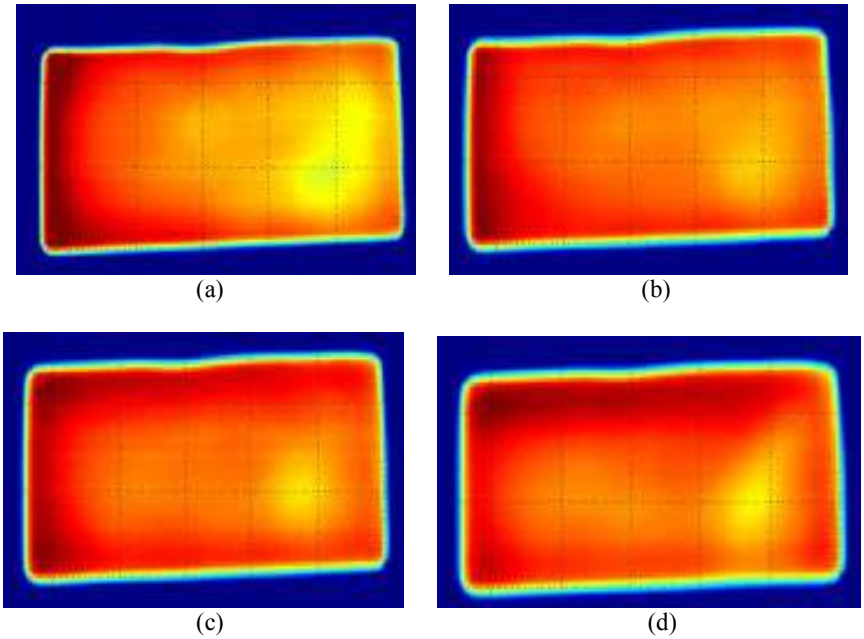

(a) (b)

(c) (d)

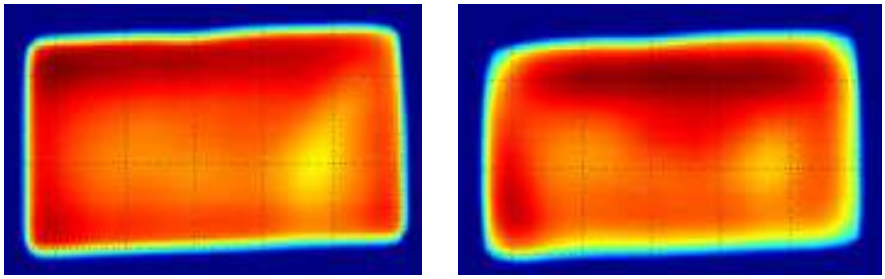

(e) (f)

Figure 7. Thermograms obtained experimentally at (a) 10 sec, (b) 15 sec, (c) 60 sec, (d) 80 sec, (e) 200 sec and (f) 450 sec after the beginning of the cooling process.

Figure 7d shows that the defects at 7.5 mm and 9 mm from the surface can only be detectable after 80 seconds and can be seem clearly after passed 200 seconds from the initial time (see Fig. 7e and f).

The experimental results showed similarity with the behavior "predicted" in the simulation. It was demonstrated that the heating temperature plays an important role in the detectability of the defects, increasing the amount of thermal radiation that the camera received from the surface. The heating method using in this work minimized the effects of the non-uniform temperature distribution, one of the main effects that affect the quality of the results.

5. FURTHER WORKS

As showed before, different types of defects have different thermal response. Therefore research concerning the possible identification of the defect type by analyzing these specific differences in temperature decay and thermal contrast curves is under way. Also, it's being examined the way of comparing quantitatively the thermal images captured experimentally and the results obtained by numerical simulation.

Another important issue that will be considered in this work is the analysis of the temperature profiles which constitute an important tool for detecting and characterize subsurface defects.

6. REFERENCES

C. Jena, N. Sarbhai, R. Mulaveesala and S. Tuli, 2006, "Pulsed Thermography Simulation: 1D, 2D and 3D Electro-Thermal Model Based Evaluation", Proc. National Seminar on Non-Destructive Evaluation, Hyderabad, 5 p.

C.R., Maliska, 1995**, "**Transferência de Calor e Mecânica dos Fluidos Computacional", Livros Técnicos e Científicos Editora S.A. Rio de Janeiro, Brasil, 453 p.

FLIR Systems AB, 2001, "ThermoCam SC500 Operator's Manual", Publ. No. 1 557 491 – Rev. B, 74 p.

FLIR Systems AB, 2001, "ThermoCam Researcher 2001 Operating Manual", version A, 131 p.

M. Pilla, Klein and X. Maldague, 2007, "Ir View 1.7.5", Free Software Foundation, Inc., Boston, MA, USA

M. Susa, C. Castanedo, X. Maldague e A. Bendada, 2007, "Pulse Thermography Applied on a Complex Structure Sample: Comparison and Analysis of Numerical and Experimental Results", IV Conferencia Panamericana de END, Buenos Aires, Argentina, 12 p.

X. Maldague, 2001, "Nondestructive Evaluation of Materials by Infrared Thermography" new revised edition, John Wiley & Sons, New Jersey, 684 p.

7. RESPONSIBILITY NOTICE

The author(s) is (are) the only responsible for the printed material included in this paper.